

## Two-channel pseudogap Kondo and Anderson models: Quantum phase transitions and non-Fermi liquids

Imke Schneider,<sup>1</sup> Lars Fritz,<sup>2</sup> Frithjof B. Anders,<sup>3</sup> Adel Benlagra,<sup>1</sup> and Matthias Vojta<sup>1</sup>

<sup>1</sup>*Institut für Theoretische Physik, Technische Universität Dresden, 01062 Dresden, Germany*

<sup>2</sup>*Institut für Theoretische Physik, Universität zu Köln, Zùlpicher Straße 77, 50937 Köln, Germany*

<sup>3</sup>*Lehrstuhl für Theoretische Physik II, Technische Universität Dortmund, Otto-Hahn-Straße 4, 44221 Dortmund, Germany*

(Received 11 August 2011; published 29 September 2011)

We discuss the two-channel Kondo problem with a pseudogap density of states  $\rho(\omega) \propto |\omega|^r$  of the bath fermions. Combining both analytical and numerical renormalization group techniques, we characterize the impurity phases and quantum phase transitions of the relevant Kondo and Anderson models. The line of stable points, corresponding to the overscreened non-Fermi-liquid behavior of the metallic  $r = 0$  case, is replaced by a stable particle-hole-symmetric intermediate-coupling fixed point for  $0 < r < r_{\max} \approx 0.23$ . For  $r > r_{\max}$ , this non-Fermi-liquid phase disappears, and instead a critical fixed point with an emergent spin-channel symmetry appears, controlling the quantum phase transition between two phases with stable spin and channel moments, respectively. We propose low-energy field theories to describe the quantum phase transitions, all being formulated in fermionic variables. We employ  $\epsilon$  expansion techniques to calculate critical properties near the critical dimensions  $r = 0$  and 1, the latter being potentially relevant for two-channel Kondo impurities in neutral graphene. We find the analytical results to be in excellent agreement with those obtained from applying Wilson's numerical renormalization group technique.

DOI: [10.1103/PhysRevB.84.125139](https://doi.org/10.1103/PhysRevB.84.125139)

PACS number(s): 75.20.Hr, 74.72.-h

### I. INTRODUCTION

The two-channel Kondo effect represents a prime example of non-Fermi-liquid behavior arising from a stable intermediate-coupling fixed point.<sup>1</sup> Theoretically, its physics is essentially understood, thanks to an exact solution by Bethe ansatz.<sup>2,3</sup> In addition, boundary conformal field theory (CFT) has proved to be a powerful technique to study the low-energy properties of the multichannel Kondo model<sup>4</sup> allowing, in particular, the calculation of exact asymptotic Green's functions.<sup>5</sup> CFT techniques have also been used to calculate exact crossover Green's functions.<sup>6</sup> Further, by means of Abelian bosonization and subsequent refermionization it has been possible to map the two-channel Kondo problem onto a resonant-level model which reduces to a free-fermion form for a particular value of exchange anisotropy.<sup>7</sup>

On the experimental side, a number of heavy-fermion materials, displaying deviations from Fermi-liquid behavior, have been speculated to realize two-channel Kondo physics arising from non-Kramers-doublet ground states of U or Pr ions.<sup>8-10</sup> However, to our knowledge, there is no unambiguous verification of these proposals. Consequently, various attempts have been made to realize the two-channel Kondo effect in nanostructures, and indeed success was reported<sup>11</sup> for a setup of a semiconductor quantum dot coupled to two reservoirs.<sup>12</sup> Very recently, signatures of two-channel Kondo behavior of magnetic adatoms on graphene have been reported,<sup>13</sup> and this motivates a discussion of two-channel Kondo impurities in nonmetallic hosts. In particular, neutral graphene realizes a pseudogap density of states (DOS)  $\rho(\omega) \propto |\omega|^r$  with  $r = 1$ , at low energies.

The single-channel pseudogap Kondo problem has been studied extensively in the context of Kondo impurities in unconventional superconductors. The main difference from the familiar metallic Kondo problem<sup>14</sup> is the absence of screening at small Kondo coupling  $J$ , leading to a quantum phase

transition upon increasing  $J$ .<sup>15-19</sup> The universality class of this phase transition changes as a function of  $r$ ,<sup>19</sup> and the relevant low-energy field theories have been worked out in detail in Refs. 20 and 21.

Although there has been speculation about two-channel Kondo physics in the context of graphene,<sup>22</sup> the two-channel pseudogap Kondo model has received little attention. A central question is about the fate and character of the non-Fermi-liquid phase at finite  $r$ . To our knowledge, the only study of the model has been reported in a brief section of Ref. 19, but there only numerical results were given for small bath exponents  $r$ .<sup>23</sup>

The purpose of this paper is to close this gap: We shall investigate the two-channel Kondo and Anderson models with a pseudogap DOS in some detail, using both analytical and numerical renormalization group (RG) techniques. Our main findings for the two-channel Kondo model are as follows:

(A) The overscreened non-Fermi-liquid (NFL) phase of the metallic two-channel Kondo model<sup>14</sup> survives for  $0 < r < r_{\max} \approx 0.23$ , albeit with an important modification: It is no longer represented by a *line* of NFL fixed points [where particle-hole (p-h) asymmetry is marginal], but instead there is only an isolated stable p-h symmetric NFL fixed point, i.e., p-h asymmetry is irrelevant for  $r > 0$ .<sup>23</sup> Furthermore, this stable NFL phase is only reached for Kondo couplings larger than a critical coupling, i.e., a boundary quantum phase transition emerges between a local-moment phase with an unscreened spin moment and the NFL phase. In contrast, for  $r > r_{\max}$  the NFL fixed point disappears, leaving only two stable phases with unscreened spin or channel (i.e., flavor) moment, respectively, which are separated by a quantum phase transition.

(B) The two-channel pseudogap Kondo physics for both  $r \lesssim 1$  and  $r \geq 1$  can be fully understood in the language of the two-channel Anderson model, by virtue of a generalization of the approach presented in Ref. 21. The low-energy field

theory describing the quantum phase transition between the phases with free spin and flavor moments is given by a level crossing of a spin doublet and a flavor doublet minimally coupled to conduction electrons. As in the single-channel pseudogap Kondo problem,  $r = 1$  is found to play the role of an upper critical dimension, where the hybridization is marginal. For  $r > 1$ , the transition is a level crossing with perturbative corrections but a nontrivial critical fixed point emerges for  $r < 1$ . This fixed point is shown to display an emergent spin-channel  $Z_2$  symmetry. As in the single-channel case, none of the quantum phase transitions is described by a Landau-Ginzburg-Wilson-type theory of a bosonic order parameter; instead all are “fermionic” in nature.

The following section gives a more detailed summary of our results.

### A. Summary of results

The two-channel Kondo model with a pseudogap host density of states can be written as  $\mathcal{H} = \mathcal{H}_K + \mathcal{H}_b$ , with

$$\begin{aligned} \mathcal{H}_K &= \sum_i [J_K \vec{S} \cdot c_{i\sigma}^\dagger(0) \vec{\tau}_{\sigma\sigma'} c_{i\sigma'}(0) + V_0 c_{i\sigma}^\dagger(0) c_{i\sigma}(0)], \\ \mathcal{H}_b &= \sum_i \int_{-\Lambda}^{\Lambda} dk |k|^r k c_{ki\sigma}^\dagger c_{ki\sigma}. \end{aligned} \quad (1)$$

Here, we have represented the bath  $\mathcal{H}_b$  by linearly dispersing chiral fermions  $c_{ki\sigma}$ , where  $i = 1, 2$  is the channel index.  $S$  is a spin-1/2  $SU(2)$  spin,  $\vec{\tau}$  is the vector of Pauli matrices, summation over repeated spin indices  $\sigma$  is implied, and  $c_{i\sigma}(0) = \int dk |k|^r c_{ki\sigma}$  is the conduction electron operator at the impurity site. The spectral density of the  $c_{i\sigma}(0)$  fermions follows the power law  $|\omega|^r$  below the ultraviolet (UV) cutoff  $\Lambda$ ; details of the density of states at high energies are irrelevant for the discussion in this paper. In addition to the Kondo coupling  $J_K$ , we have also included a potential scatterer of strength  $V_0$  at the impurity site which will be used to tune p-h asymmetry. (An asymmetry of the high-energy part of the DOS would have a net effect similar to nonzero  $V_0$ ; for simplicity we will assume in the following that the DOS is p-h symmetric.)

As we shall show below, a comprehensive analysis requires us to consider—in addition to the two-channel Kondo model—the two-channel Anderson model, commonly written as  $\mathcal{H} = \mathcal{H}_A + \mathcal{H}_b$  with<sup>8</sup>

$$\begin{aligned} \mathcal{H}_A &= \varepsilon_s \sum_{\sigma} |\sigma\rangle\langle\sigma| + \varepsilon_q \sum_i |i\rangle\langle i| \\ &+ g_0 \sum_{k\sigma i} (|\sigma\rangle\langle i| c_{ki\sigma} + \text{H.c.}) + V_0 \sum_{\sigma i} c_{i\sigma}^\dagger(0) c_{i\sigma}(0). \end{aligned} \quad (2)$$

Here, the isolated impurity has four states, i.e., a spin doublet  $|\sigma\rangle = |\uparrow\rangle, |\downarrow\rangle$  and a channel doublet  $|i\rangle = |1\rangle, |2\rangle$ . Their mass difference  $\varepsilon_0 \equiv \varepsilon_s - \varepsilon_q$  will play a role as a tuning parameter of the quantum phase transition.

For a given value of the bath exponent  $r$ , the two-channel pseudogap Kondo and Anderson models display common RG fixed points. The phase diagram and critical behavior depend on  $r$ , with  $r = 0$ ,  $r = r_{\max}$ , and  $r = 1$  marking qualitative changes and playing the role of critical “dimensions.” In the following, we describe our central results for the phase diagrams and RG flows, which are partially consistent<sup>23</sup>

with the ones reported in Ref. 19. The qualitative behavior is visualized in the RG flow diagrams in Fig. 1 for the two-channel Kondo model and Fig. 2 for the two-channel Anderson model, respectively. In the latter case, a cut through the RG flow at  $V_0 = 0$  is shown.

The metallic case  $r = 0$  has been studied extensively, and a line of infrared-stable NFL fixed points governs the behavior at any finite coupling—this is the well-known two-channel (or overscreened) Kondo effect. In the two-channel Anderson model, this line of fixed points can be accessed by varying  $\varepsilon_0$ , i.e., initial parameters with different  $\varepsilon_0$  flow to different fixed points along this line<sup>25</sup>—note that this flow leaves the  $v = 0$  plane for  $\varepsilon \neq 0$  (dashed lines in Fig. 2; all symbols denote the renormalized coupling parameter).

For positive  $r$  with  $0 < r < r_{\max}$ , the line of stable NFL fixed points collapses to an isolated p-h-symmetric NFL fixed point. In addition, the local-moment (LM) fixed point of an unscreened spin moment now becomes stable. In the language of the Kondo model, LM corresponds to  $j = v = 0$ , while in the Anderson model it corresponds to  $\varepsilon = -\infty$ ,  $g = 0$ . The phase transition between the LM and NFL fixed points is controlled by a p-h-symmetric critical (SCR) fixed point; note that this p-h-symmetric fixed point is located outside the  $v = 0$  plane for the Anderson model shown in Fig. 2. As  $r \rightarrow 0$  SCR approaches LM and the critical behavior of SCR is perturbatively accessible for small Kondo coupling  $J_K$ . The phase diagram of the Anderson model is mirror symmetric, i.e., there exists also an unscreened channel (or flavor) local-moment fixed point  $LM'$  at  $\varepsilon = \infty$ ,  $g = 0$ ,<sup>24</sup> and a corresponding critical intermediate-coupling fixed point  $SCR'$  at positive  $\varepsilon$ .

As  $r \rightarrow r_{\max}$  SCR approaches NFL, and the two fixed points disappear for  $r > r_{\max}$ . In the p-h-symmetric Kondo model, this implies that the flow is toward LM for any value of  $j$ , but for large asymmetries,  $LM'$  may be reached.<sup>24</sup> In the Anderson model, the hybridization  $g$  remains relevant at  $\varepsilon = 0$  for  $r_{\max} < r < 1$ , but the flow is toward a single unstable intermediate-coupling asymmetric critical (ACR) fixed point in the  $v = 0$  plane, i.e., ACR is p-h asymmetric, but is invariant under the  $Z_2$  transformation (4). At finite coupling, the transition between the two stable fixed points LM and  $LM'$  is controlled by ACR.

Finally, as  $r \rightarrow 1$  ACR moves toward  $g \rightarrow 0$  and for  $r \geq 1$  the phase transition becomes a level crossing with perturbative corrections, controlled by the free-impurity fixed point (FImp) at  $\varepsilon = 0, g = 0$ .

### B. Outline

The bulk of this paper is organized as follows: We start in Sec. II by discussing the relevant impurity models, suitably generalized to higher degeneracies, along with their underlying symmetries. In Sec. III we present selected results from Wilson’s numerical renormalization group (NRG) for the two-channel pseudogap Anderson and Kondo models which illustrate the content of the flow diagrams in Figs. 1 and 2. In particular, we show properties of the nontrivial intermediate-coupling fixed points as functions of the bath exponent  $r$ . Sections IV and V are devoted to the  $\epsilon$  expansion studies of the critical fixed points, using the variables of the Kondo model

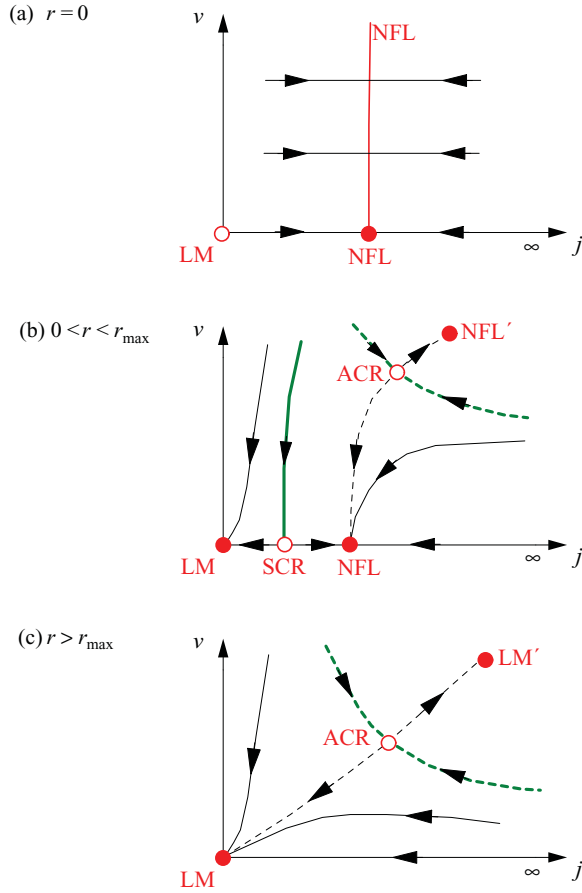


FIG. 1. (Color online) Schematic RG flow diagrams for the two-channel Kondo model with a pseudogap DOS  $\rho(\omega) \propto |\omega|^r$ . The horizontal axis denotes the renormalized Kondo coupling  $j$ , and the vertical axis is the renormalized potential scattering  $v$ , representing particle-hole asymmetry. Dashed flow lines symbolize a flow out of the plane shown here. The thick lines correspond to continuous boundary phase transitions; the full (open) circles are stable (unstable) fixed points. (a)  $r=0$ , i.e., the familiar metallic case. For any finite  $j$  the flow is toward the line of NFL fixed points, describing two-channel non-Fermi-liquid behavior. (b)  $0 < r < r_{\max}$ : p-h asymmetry is irrelevant in the NFL phase, such that the line of fixed points is replaced by a single p-h-symmetric NFL fixed point. The local-moment fixed point LM is stable and separated from NFL by a p-h-symmetric critical (SCR) fixed point. For  $r \rightarrow 0$  ( $r \rightarrow r_{\max}$ ), SCR approaches LM (NFL). Depending on microscopic details, a second NFL' phase may be reached at large couplings and asymmetries, separated by a critical ACR fixed point; see text. (c)  $r \geq r_{\max}$ : The NFL phase disappears, and the only phase transition is between LM and LM', the latter representing a free-channel (i.e., flavor) moment. This transition is controlled by ACR. Note that the character of this transition changes at  $r = 1$ , where ACR merges with FImp; see text.

(Sec. IV) and those of the Anderson model (Sec. V). The latter provide access to the physics near the upper critical dimension  $r = 1$ . Concluding remarks close the paper. A discussion of the Majorana representation of the two-channel Kondo problem and its fate in the presence of a pseudogap DOS is relegated to the Appendix.

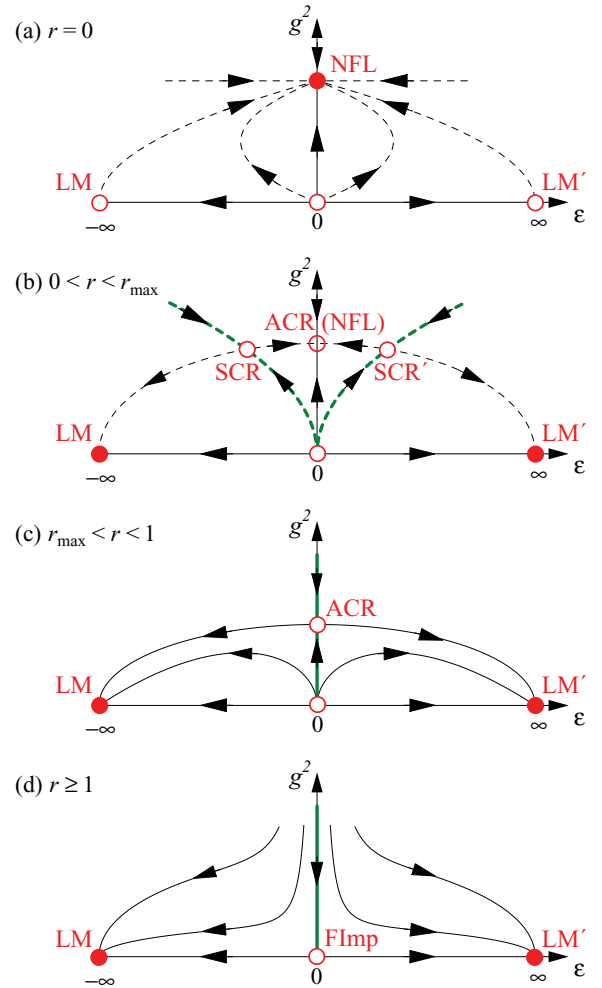


FIG. 2. (Color online) As Fig. 1, but for the two-channel Anderson model. The horizontal axis denotes the energy difference  $\varepsilon$  between spin and flavor impurity levels, and the vertical axis is the renormalized hybridization  $g$ . The diagrams represent cuts, taken at  $v = 0$ , through the full RG flow. The flow diagrams are mirror symmetric by virtue of the  $Z_2$  transformation (4). (a)  $r=0$ . The line of NFL fixed points, describing two-channel non-Fermi-liquid behavior crosses the  $v = 0$  plane at  $\varepsilon = 0$ . (b)  $0 < r < r_{\max}$ : The fixed points LM, LM' are stable, corresponding to unscreened spin and flavor moments, respectively. Within the  $v = 0$  plane, NFL is replaced by ACR, whereas two isolated p-h-symmetric NFL and NFL' fixed points exist outside this plane. The transitions to NFL and NFL' are controlled by the p-h-symmetric SCR and SCR' fixed points (located outside the  $v = 0$  plane). (c)  $r_{\max} \leq r < 1$ :  $g$  is still relevant at  $\varepsilon = 0$ . However, NFL is now replaced by a single unstable fixed point (ACR) located in the  $v = 0$  plane. At finite  $g$ , the transition between the two stable fixed points LM and LM' is controlled by ACR. (d)  $r \geq 1$ :  $g$  is irrelevant, and the only transition is a level crossing (with perturbative corrections) occurring at  $g = \varepsilon = 0$ , i.e., at the free-impurity fixed point (FImp).

## II. MODELS, SYMMETRIES, AND MAPPINGS

### A. Anderson model

The two-channel Anderson model can be understood as describing the level crossing between two impurity doublets— one spin doublet and one channel (i.e., flavor) doublet— coupled to conduction electrons via a hybridization term. The

model features an  $SU(2)_{\text{spin}} \times SU(2)_{\text{flavor}}$  symmetry. This can be straightforwardly generalized to  $SU(N)_{\text{spin}} \times SU(K)_{\text{flavor}}$  symmetry, where  $N$  is the number of spin degrees of freedom and  $K$  the number of flavors. The Hamiltonian can be written as

$$\begin{aligned} \mathcal{H}_A = & \mathcal{H}_b + \varepsilon_s \sum_{\sigma} |\sigma\rangle\langle\sigma| + \varepsilon_q \sum_{\alpha} |\bar{\alpha}\rangle\langle\bar{\alpha}| \\ & + g_0 \sum_{k\alpha\sigma} (|\sigma\rangle\langle\bar{\alpha}| c_{k\alpha\sigma} + \text{H.c.}) + V_0 \sum_{\alpha\sigma} c_{\alpha\sigma}^{\dagger}(0) c_{\alpha\sigma}(0). \end{aligned} \quad (3)$$

Here, the conduction electrons  $c_{k\alpha\sigma}$  transform under a fundamental representation of  $SU(N)$  and  $SU(K)$  and carry the corresponding spin  $\sigma$  and flavor  $\alpha$  indices.  $\bar{\alpha}$  indicates a transformation behavior according to the conjugate representation. For  $N = 2$ ,  $K = 1$ , the Hamiltonian in Eq. (3) describes the single-channel Anderson model in the limit of infinite Coulomb repulsion ( $U = \infty$ ), studied using the RG in Ref. 21. In the case of a metallic host,  $r = 0$ , the multichannel Anderson model is integrable and has been solved using the Bethe ansatz<sup>25–27</sup> and the numerical RG method.<sup>28</sup>

The metallic two-channel Anderson model, i.e.,  $N = 2$ ,  $K = 2$ , has been proposed as a model for the observed non-Fermi-liquid behavior of the heavy-fermion superconductor  $U\text{Be}_{13}$ .<sup>29</sup> In this scenario, the  $5f^2$  ground state of the U ion is identified as the  $\Gamma_3$  nonmagnetic quadrupolar doublet, while the first excited state is the  $5f^3$   $\Gamma_7$  magnetic doublet.<sup>8</sup> This then can promote a quadrupolar Kondo effect where the quadrupolar doublet is quenched by the hybridization with  $\Gamma_8$  conduction electrons which carry both magnetic and quadrupolar degrees of freedom.<sup>9</sup> In particular, since the energy difference between the two doublets appears to be small, a mixed-valence state is likely, requiring the study of the full Anderson model.<sup>30</sup> Consequently, the model (3) with a pseudogap DOS is of potential relevance, not only to two-channel impurities in graphene, but also to quadrupolar Kondo impurities in unconventional superconductors.

The Anderson model (3) is *not* particle-hole symmetric for any value of  $V_0$ , due to the asymmetric structure of the impurity. However, p-h symmetry is dynamically restored for  $0 < r < r_{\text{max}}$  both inside the NFL and NFL' phases and at the critical SCR and SCR' fixed points; see Fig. 1.

Interestingly, for  $N = K$  and a p-h-symmetric bath, the Anderson model displays a spin-channel symmetry, i.e., is invariant under the combined transformation

$$\begin{aligned} |\sigma\rangle & \leftrightarrow |\bar{\alpha}\rangle, & c_{k\alpha\sigma} & \leftrightarrow c_{k\alpha\sigma}^{\dagger}, \\ \varepsilon_0 & \leftrightarrow -\varepsilon_0, & V_0 & \leftrightarrow -V_0. \end{aligned} \quad (4)$$

Here, the spin-carrying impurity states are transformed into the flavor-carrying states and vice versa, i.e., the two  $SU(N)$  sectors are interchanged, together with a p-h transformation.

### B. Kondo models

The Anderson model (3) has two Kondo limits. On the one hand, for  $\varepsilon_0 = \varepsilon_s - \varepsilon_q \rightarrow -\infty$  it maps to a  $K$ -channel  $SU(N)_{\text{spin}}$  Kondo model, where a spinful impurity is coupled

to  $K$  channels of conduction electrons. For  $N = 2$  the Hamiltonian reads

$$\begin{aligned} \mathcal{H}_K = & \mathcal{H}_b + J_K \vec{S} \cdot \sum_{\alpha\sigma\sigma'} c_{\alpha\sigma}^{\dagger}(0) \vec{\tau}_{\sigma\sigma'} c_{\alpha\sigma'}(0) \\ & + V_0 \sum_{\alpha\sigma} c_{\alpha\sigma}^{\dagger}(0) c_{\alpha\sigma}(0), \end{aligned} \quad (5)$$

where  $\vec{S}$  is a spin-1/2  $SU(2)$  spin and  $\sigma, \sigma' = \uparrow, \downarrow$ . For  $N > 2$  the impurity spin is in a fundamental representation of  $SU(N)$ . The parameters of the Kondo model (5) are related to that of the  $V_0 = 0$  Anderson model (3) through

$$J_K = N V_0 = \frac{g_0^2}{|\varepsilon_0|}. \quad (6)$$

The Kondo limit is reached by taking  $\varepsilon_0 \rightarrow -\infty$ ,  $g_0 \rightarrow \infty$ , keeping  $J_K$  fixed. Note that a potential scattering term is always generated.

On the other hand, for  $\varepsilon_0 \rightarrow +\infty$  the Anderson model can be mapped to an  $N$ -channel  $SU(K)_{\text{flavor}}$  Kondo model, where  $\vec{S}$  represents an  $SU(K)$  impurity which is screened by the  $N$  spin degrees of freedom of the conduction electrons. This multichannel flavor Kondo effect is relevant, e.g., to the charging process of a quantum box, where the flavor degree of freedom is taken by the physical charge.<sup>31,32</sup>

We note that the multichannel Kondo model cannot be obtained by a Schrieffer-Wolff transformation from any standard Anderson model (i.e., one written with free-electron operators and local Coulomb interaction).

### C. Large- $N$ limit

The  $SU(N)$  multichannel Kondo model can be solved in a dynamic large- $N$  limit for both fully symmetric (bosonic) and fully antisymmetric (fermionic) representations of  $SU(N)$ .<sup>33</sup> The fermionic version of this solution, with  $K = \gamma N$  and  $K, N \rightarrow \infty$ , has been generalized to the pseudogap case.<sup>34</sup> The large- $N$  phase diagram, Fig. 1 of Ref. 34, is similar to that of the  $N = K = 2$  case, i.e., the overscreened non-Fermi-liquid phase survives for small  $r$ , where it is reached for a certain range of couplings only, while this phase disappears for larger  $r \lesssim 1$ . Also, all leading anomalous dimensions vanish for  $r > 1$ .

Two qualitative differences between the large- $N$  scenario and  $N = K = 2$  are worth noting: (i) The critical ‘‘dimension’’  $r_{\text{max}}$  of  $N = K = 2$  splits into two in the large- $N$  limit, with their values and the detailed behavior depending upon the value of  $\gamma$ . (ii) The quantum phase transitions in the large- $N$  limit are governed by *lines* of fixed points, with continuously varying exponents as functions of the particle-hole asymmetry, in contrast to the isolated critical fixed points SCR and ACR in Figs. 1 and 2. This implies that the scaling dimension of  $V_0$  vanishes at criticality as  $N \rightarrow \infty$ , rendering the large- $N$  limit partially singular. We therefore refrain from a detailed discussion of the models (3) and (5) for large  $N$ .

### D. Observables

In the bulk of the paper, we will focus on a few important observables which characterize the phases and phase transitions of the impurity models under consideration.

Those include the correlation-length exponent, the impurity entropy, various susceptibilities, and the conduction-electron  $T$  matrix (or impurity spectral function). Their definition is standard, and we refer the reader to Refs. 19,21,35–37 for a detailed exposition. Here we only summarize a few key aspects.

The spin susceptibilities  $\chi^{(\text{spin})}$  are obtained by coupling external magnetic fields to both the bulk and impurity degrees of freedom as explained in detail in Ref. 37. For the impurity part, here, this reads

$$-H_{\text{imp},i}|\sigma\rangle\lambda_{\sigma\sigma'}^i\langle\sigma'|, \quad (7)$$

where  $H_{\text{imp},i}$  is the magnetic field coupling to the impurity spin, while the  $\lambda_{\sigma\sigma'}^i$  with  $i = 1, N - 1$  are generators of  $SU(N)$ . In the following, we exploit the  $SU(N)$  symmetry and evaluate the corresponding susceptibility tensor only in the one-direction, choosing the representation  $\lambda_{\sigma\sigma'}^1 = \frac{1}{2}(\delta_{\sigma,1}\delta_{\sigma',1} - \delta_{\sigma,2}\delta_{\sigma',2})$ .<sup>38</sup> We proceed as usual by calculating the magnetic susceptibilities via the corresponding linear response functions. Note that the impurity susceptibility is composed of

$$\chi_{\text{imp}}(T) = \chi_{\text{imp,imp}} + 2\chi_{\text{b,imp}} + (\chi_{\text{b,b}} - \chi_{\text{b,b}}^0), \quad (8)$$

where  $\chi_{\text{imp,imp}}$  is the response to  $H_{\text{imp}}$ ,  $\chi_{\text{b,b}}$  measures the bulk response to the field applied to the bulk,  $\chi_{\text{b,imp}}$  are the cross terms, and  $\chi_{\text{b,b}}^0$  denotes the bulk response in the absence of the impurity. The flavor susceptibilities  $\chi^{(\text{flavor})}$  can be defined in the Anderson model in analogy to the spin susceptibilities (i.e., with  $\sigma \rightarrow \alpha$ ).

Owing to symmetries, the total magnetization in both the spin and flavor sectors is conserved. This implies that the impurity contributions to the spin and flavor susceptibilities,  $\chi_{\text{imp}}^{(\text{spin})}$  and  $\chi_{\text{imp}}^{(\text{flavor})}$ , do not acquire anomalous exponents at the intermediate-coupling fixed points, but instead obey Curie laws with (in general) fractional prefactors. In contrast, the local spin and flavor susceptibilities follow anomalous power laws,  $\chi_{\text{loc}}^{(\text{spin})} \propto T^{-1+\eta_\chi^{(\text{spin})}}$  and  $\chi_{\text{loc}}^{(\text{flavor})} \propto T^{-1+\eta_\chi^{(\text{flavor})}}$ , with universal  $r$ -dependent exponents  $\eta_\chi$ . We note that a direct calculation of both susceptibilities is possible only in the Anderson model, as the Kondo limit suppresses the local piece of one of the susceptibilities. To shorten notation, we employ the convention  $\chi \equiv \chi^{(\text{spin})}$  and  $\eta_\chi \equiv \eta_\chi^{(\text{spin})}$  in the following.

Similar to  $T\chi_{\text{imp}}^{(\text{spin,flavor})}$ , the impurity entropy approaches a universal fractional value as  $T \rightarrow 0$ . The conduction-electron  $T$  matrix, on the other hand, follows an anomalous power law similar to that of the local susceptibility,  $T(\omega) \propto \omega^{-1+\eta_r}$ .

At the non-Fermi-liquid fixed point of the familiar metallic two-channel Kondo model ( $r = 0$ ), power laws are replaced by logarithms,  $\chi_{\text{loc}}, \chi_{\text{imp}} \propto \ln 1/T$ ; this also implies that the prefactor of the leading Curie term in  $\chi_{\text{imp}}$  vanishes due to an exact compensation.

### III. SELECTED NUMERICAL RESULTS

The NRG technique<sup>39</sup> is ideally suited to study properties of quantum impurity models, including non-Fermi-liquid phases and quantum phase transitions. Initial NRG results for the two-channel pseudogap Kondo model were shown in Ref. 19. Here we extend and complement this early analysis by NRG results for the two-channel ( $N = K = 2$ ) Anderson model.

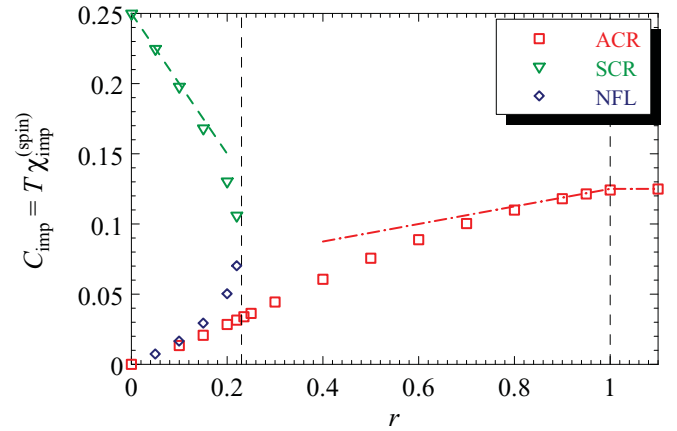


FIG. 3. (Color online) NRG results for the impurity susceptibility  $T\chi_{\text{imp}}$  at the intermediate-coupling fixed points ACR ( $\square$ ), SCR ( $\triangle$ ), and NFL ( $\diamond$ ). Also shown are the results from the renormalized perturbation theory of the Kondo model, which allows us to access SCR near  $r = 0$  [Sec. IV, Eq. (14), dashed], and those from the Anderson model, appropriate for ACR for  $r \lesssim 1$  [Sec. V, Eq. (49), dash-dotted]. The SCR data are partially taken from Ref. 19. The vertical dashed lines indicate the critical dimensions  $r = r_{\text{max}}$  and  $r = 1$ .

We perform explicit calculations for a bath density of states  $\rho(\omega) = (1+r)/(2D)|\omega/D|^r \Theta(D^2 - \omega^2)$  with  $D = 1$ . Unless otherwise noted, we employ NRG parameters<sup>39</sup>  $\Lambda = 6$  and  $N_s = 600$ .

The qualitative behavior of the two-channel Anderson model is summarized in the flow diagram in Fig. 2. In addition to the stable LM and LM' phases, these flow diagrams feature three nontrivial fixed points: the stable NFL and NFL' fixed points, and the critical fixed points SCR, SCR', and ACR. Some of their key properties are summarized in Figs. 3 and 4, which show the numerically determined impurity contributions to the spin susceptibility and the entropy, respectively, together with analytical results obtained from the  $\epsilon$  expansion of Secs. IV and V. These plots nicely show that NFL and SCR approach

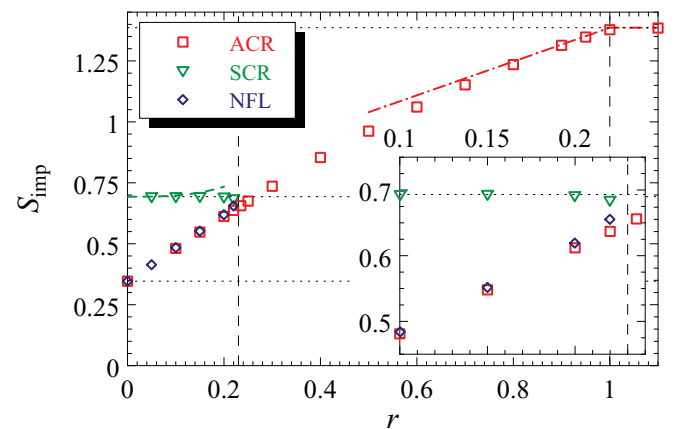


FIG. 4. (Color online) As Fig. 3, but for the impurity entropy  $S_{\text{imp}}$ . The perturbative expansions are in Eq. (15) (dashed) and Eq. (53) (dash-dotted). The dotted horizontal lines correspond to  $S_{\text{imp}} = 0.5 \ln 2$ ,  $\ln 2$ , and  $\ln 4$ . The inset shows a zoom onto the region  $r \lesssim r_{\text{max}}$ .

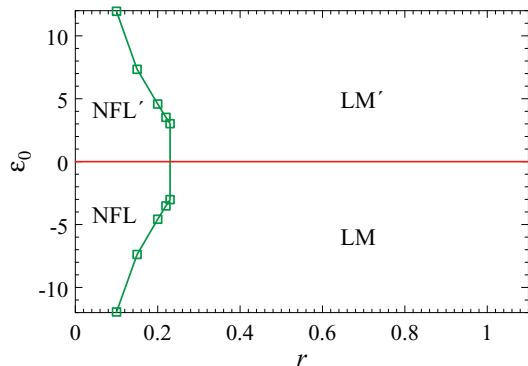


FIG. 5. (Color online) Phase diagram of the two-channel Anderson model as a function of the energy difference  $\varepsilon_0$  and the bath exponent  $r$ , keeping  $g_0^2 = 4$  fixed. The discontinuous change at  $r = r_{\max}$  is apparent.

each other as  $r \rightarrow r_{\max}$ , while ACR evolves continuously near  $r_{\max}$ . The fixed-point properties also show that SCR approaches LM as  $r \rightarrow 0$ , with  $T\chi_{\text{imp}} \rightarrow 1/4$  and  $S_{\text{imp}} \rightarrow \ln 2$ , and ACR approaches FImp as  $r \rightarrow 1$ , with  $T\chi_{\text{imp}} \rightarrow 1/8$  and  $S_{\text{imp}} \rightarrow \ln 4$ . Further, the stable NFL fixed point follows  $T\chi_{\text{imp}} \rightarrow 0$  and  $S_{\text{imp}} \rightarrow 0.5 \ln 2$  as  $r \rightarrow 0$ —the well-known properties of the metallic two-channel Kondo problem.

The disappearance of both NFL and SCR upon increasing  $r$  beyond  $r_{\max}$  implies a *discontinuous* evolution of the phase diagram as a function of  $r$ . In Fig. 5 we present a cut through the phase diagram of the Anderson model at fixed  $g_0$  which illustrates this fact. We note that such a discontinuous evolution occurs if a stable intermediate-coupling fixed point disappears (here NFL); in contrast, if a trivial fixed point changes its nature from stable to unstable, the evolution is continuous, as in the single-channel pseudogap Kondo model.

The correlation-length exponents  $\nu$  are displayed in Fig. 6, illustrating that  $r = 0$  and  $r_{\max}$  play the role of lower critical dimensions for the p-h-symmetric transition controlled by

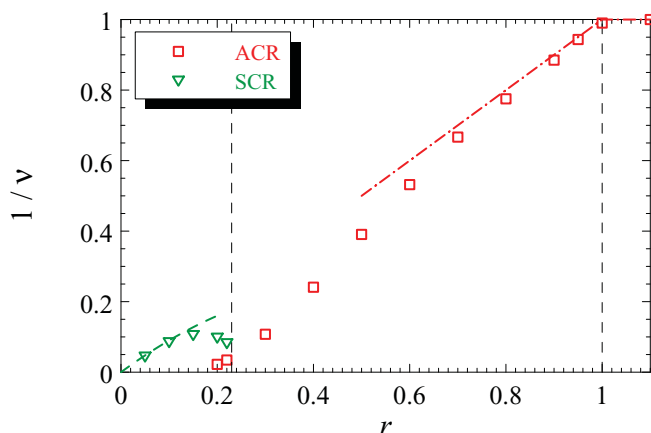


FIG. 6. (Color online) Inverse correlation-length exponent  $1/\nu$  obtained from NRG calculations for the ACR ( $\square$ ) and SCR ( $\triangle$ ) critical points, together with the analytical RG results from the expansions in  $r$  [Sec. IV, Eq. (12), dashed] and in  $(1-r)$  [Sec. V, Eq. (38), dash-dotted]. Note that  $\nu$  of ACR becomes very large for small  $r$ —this corresponds to the extremely slow flow from ACR to NFL for  $0 < r < r_{\max}$ .

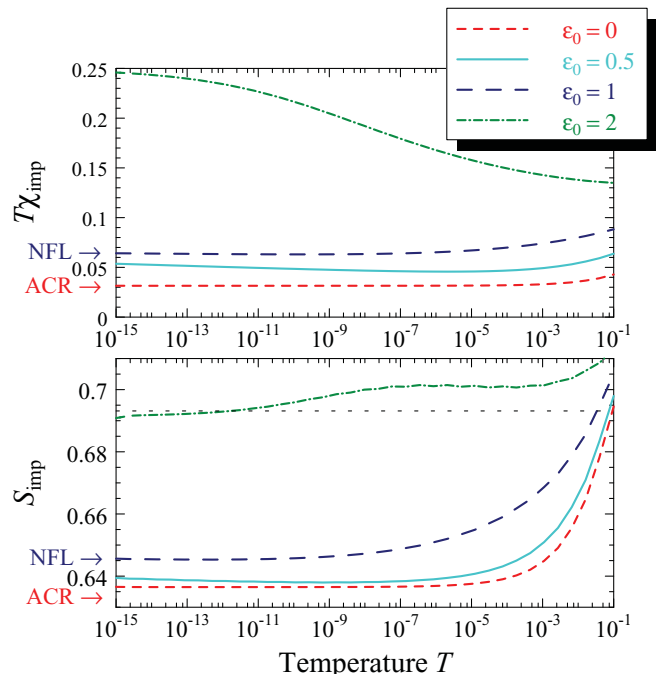


FIG. 7. (Color online) NRG results for (a) the impurity susceptibility  $T\chi_{\text{imp}}$  and (b) the impurity entropy  $S_{\text{imp}}$  of the two-channel Anderson model at  $r = 0.22$ . Parameter values are  $g_0^2 = 2$  and  $\varepsilon_0 = 0$  (dashed), 0.5 (solid), 1 (long-dashed), and 2 (dash-dotted). Both  $\varepsilon_0 = 0.5$  and 1 are located in the NFL phase while  $\varepsilon_0 = 2$  corresponds to the LM phase. The  $\varepsilon_0 = 0.5$  curves show the flow from ACR to NFL upon lowering  $T$ , where in particular the impurity entropy *increases* along the RG flow. (The flow is too slow to reach its fixed point within the accessible temperature range.)

SCR, with  $\nu \rightarrow \infty$ , whereas  $r = 1$  is the upper critical dimension of the ACR transition, with  $\nu = 1$  for all  $r > 1$  (and logarithmic corrections at  $r = 1$ ).

Figure 7 shows the temperature evolution of both  $T\chi_{\text{imp}}$  and  $S_{\text{imp}}$  for  $r = 0.22$ , i.e., slightly below  $r_{\max}$ . Here, the flow from ACR to NFL [compare Fig. 1(b)] is nicely visible at  $\varepsilon_0 = 0.5$  where both  $T\chi_{\text{imp}}$  and  $S_{\text{imp}}$  increase along the RG flow. (The large value of  $\nu$  at ACR renders the flow very slow.) Remarkably, the fact that  $S_{\text{ACR}} < S_{\text{NFL}}$  violates the so-called  $g$ -theorem,<sup>40</sup> which states that the impurity entropy should decrease along the flow. As this theorem applies to conformally invariant systems only, we conclude that the fixed points under consideration are not described by a conformally invariant theory. (The same conclusion can be drawn for the quantum phase transitions of the single-channel pseudogap Kondo problem; see Ref. 21. Also, such “uphill flow” may occur in models with long-range interactions; see e.g. Ref. 41.)

#### IV. WEAK-COUPLING EXPANSION FOR THE MULTICHANNEL KONDO MODEL

In this section we review the standard weak-coupling expansion<sup>42</sup> for the multichannel SU(2) Kondo model in Eq. (5), extended to a pseudogapped bath density of states.<sup>15,19</sup> As we show below, this expansion captures the properties of the critical fixed point SCR at small  $r$ . In principle, it also allows

one to access the stable NFL fixed point, but this requires a particular limit of large  $K$  which does not allow quantitative results for the  $K = 2$  case of interest to be extracted.

RG equations can be derived, e.g., using the field-theoretic scheme<sup>43,44</sup> where logarithmic divergencies, occurring for  $r = 0$ , are replaced by poles in  $r$  by means of dimensional regularization. Doing so will cause  $r$  to enter only in the bare scaling dimension of the couplings. To two-loop order, the equations for the renormalized couplings  $j$  and  $v$  read

$$\beta(j) = rj - j^2 + \frac{K}{2}j^3, \quad \beta(v) = rv, \quad (9)$$

where  $K$  is the number of equivalent screening channels. Importantly, there is no renormalization of  $v$ , a result which persists to higher orders.

Apart from the LM fixed point,  $j = v = 0$ , the function  $\beta(j)$  in Eq. (9) yields two further zeros, given by  $j = (1 \pm \sqrt{1 - 2Kr})/K$ . The smaller one corresponds to an infrared unstable fixed point at

$$j^* = r + \frac{K}{2}r^2 + O(r^3), \quad v^* = 0, \quad (10)$$

which can be perturbatively controlled for  $r \rightarrow 0$  and any  $K$ . We label this fixed point by SCR. As  $r \rightarrow 0$  SCR approaches LM. The larger zero predicts an infrared stable fixed point at

$$j^* = \frac{2}{K} - r - \frac{K}{2}r^2 + O(r^3), \quad v^* = 0. \quad (11)$$

Strictly speaking, this fixed point is perturbatively accessible only if the limits  $r \rightarrow 0$  and  $K \rightarrow \infty$  are taken either in this order (this corresponds to  $r = 0$ ) or together such that  $Kr$  is kept fixed. For  $r = 0$ , where  $v$  is marginal, this zero of  $\beta(j)$  is commonly associated with the line of stable non-Fermi-liquid fixed points of the multichannel Kondo model, which exists for all  $K \geq 2$ . For  $r > 0$  now  $v$  becomes irrelevant, in agreement with our numerical results<sup>23</sup> which show that the NFL line of fixed points shrinks to a single p-h-symmetric NFL fixed point, Fig. 1.

### A. Observables near criticality

The properties of the p-h-symmetric critical fixed point SCR, existing for  $0 < r < r_{\max}$ , can be determined in analogy to the single-channel case, with explicit calculations given, e.g., in Ref. 37. Expanding the  $\beta$  function (9) around the fixed point value (10) yields the correlation-length exponent  $\nu$ :

$$\frac{1}{\nu} = r - \frac{K}{2}r^2 + O(r^3). \quad (12)$$

The leading-order perturbative corrections to the impurity susceptibility and entropy are given by

$$\Delta(T\chi_{\text{imp}}) = -\frac{Kj}{4}, \quad \Delta S_{\text{imp}} = \frac{3\pi^2 \ln 2}{8} K j^2 r. \quad (13)$$

Inserting the fixed-point value  $j^*$  (10), we obtain

$$T\chi_{\text{imp}} = \frac{1}{4}(1 - Kr) + O(r^2), \quad (14)$$

$$S_{\text{imp}} = \ln 2 \left( 1 + \frac{3\pi^2}{8} Kr^3 \right) + O(r^5). \quad (15)$$

The anomalous exponent of the local susceptibility is given by  $\eta_\chi = Kj^2$  to leading order, which evaluates to

$$\eta_\chi = Kr^2 + O(r^3). \quad (16)$$

Finally, the  $T$  matrix exponent is  $\eta_T = 1 - j$  (with no factor of  $K$ , as the  $T$  matrix describes the scattering of electrons from one specific channel), resulting in

$$\eta_T = 1 - r. \quad (17)$$

Note that this result is exact.<sup>21</sup>

## V. HYBRIDIZATION EXPANSION FOR THE MULTICHANNEL ANDERSON MODEL

We now turn our attention to the multichannel Anderson model. As we show below, the variables of the Anderson model will allow us to obtain an essentially complete understanding of the multichannel pseudogap Kondo effect for both  $r \lesssim 1$  and  $r \geq 1$ . A similar conclusion was reached for the single-channel case in Refs. 20 and 21, and—on a technical level—our work represents a generalization of the calculation for the infinite- $U$  Anderson model in Ref. 21.

### A. Trivial fixed points

For vanishing hybridization  $g_0$ , the multichannel Anderson model (3) features three trivial fixed points: for  $\varepsilon_0 < 0$  the ground state is the spinful  $N$ -fold-degenerate local-moment state (LM) and, analogously, for  $\varepsilon_0 > 0$  it is the  $K$ -fold-degenerate flavor local-moment state (LM'). In these cases the impurity entropy equals  $\ln N$  and  $\ln K$ , respectively. For  $\varepsilon_0 = 0$  there are  $(N + K)$  degenerate impurity states; we refer to this as the free-impurity fixed point (FImp), with entropy  $\ln(N + K)$ . The impurity spin susceptibilities are

$$T\chi_{\text{imp}}^{(\text{spin})} = \begin{cases} \frac{1}{2N}, & \text{LM,} \\ \frac{1}{2(N+K)}, & \text{FImp,} \\ 0, & \text{LM'.} \end{cases} \quad (18)$$

The corresponding values of  $T\chi_{\text{imp}}^{(\text{flavor})}$  follow via Eq. (4) from LM  $\leftrightarrow$  LM'. The hybridization term  $g_0$  is irrelevant at LM and LM' for  $r > 0$ .

### B. Hybridization expansion and upper critical dimension

In the following we perform an expansion around the FImp fixed point, i.e., around  $\varepsilon_0 = 0$ ,  $g_0 = 0$ . The impurity states are represented by bosonic operators  $b_\alpha^\dagger$  for  $\alpha = 1, \dots, K$  and fermionic operators  $f_\sigma$  for  $\sigma = 1, \dots, N$ . Single occupancy of the localized levels is enforced by the Hilbert space constraint  $\hat{Q} \equiv \sum_\alpha b_\alpha^\dagger b_\alpha + \sum_\sigma f_\sigma^\dagger f_\sigma = 1$  which will be implemented using a chemical potential  $\lambda_0 \rightarrow \infty$ . Observables are then calculated as<sup>45,46</sup>

$$\langle \hat{O} \rangle = \lim_{\lambda_0 \rightarrow \infty} \frac{\langle \hat{Q} \hat{O} \rangle_{\lambda_0}}{\langle \hat{Q} \rangle_{\lambda_0}}, \quad (19)$$

where  $\langle \dots \rangle_{\lambda_0}$  denotes the thermal expectation value in the presence of the chemical potential  $\lambda_0$ .

Furthermore, we need to introduce chemical-potential counterterms which cancel the shift of the critical point

occurring in perturbation theory upon taking the limit of infinite UV cutoff. Technically, this shift arises from the real parts of the self-energies of the  $b_{\bar{\alpha}}$  and  $f_{\sigma}$  particles. We introduce the counterterms as additional chemical potentials for the auxiliary particles,

$$\delta\lambda_b b_{\bar{\alpha}}^{\dagger} b_{\bar{\alpha}}, \quad \delta\lambda_f f_{\sigma}^{\dagger} f_{\sigma}. \quad (20)$$

The  $\delta\lambda_{b,f}$  have to be determined order by order in an expansion in  $g_0$ . Note that counterterm contributions in observables in general enter both numerator and denominator in Eq. (19).

In the path integral form the model (3) is written as

$$\begin{aligned} \mathcal{S} = \int_0^{\beta} d\tau & \left[ \bar{f}_{\sigma}(\partial_{\tau} + \lambda_0 + \varepsilon_s + \delta\lambda_f) f_{\sigma} \right. \\ & + \bar{b}_{\bar{\alpha}}(\partial_{\tau} + \lambda_0 + \varepsilon_q + \delta\lambda_b) b_{\bar{\alpha}} + g_0(\bar{f}_{\sigma} b_{\bar{\alpha}} c_{\alpha\sigma}(0) + \text{c.c.}) \\ & \left. + \int_{-\Lambda}^{\Lambda} dk |k|^r \bar{c}_{k\alpha\sigma}(\partial_{\tau} + k) c_{k\alpha\sigma} \right], \quad (21) \end{aligned}$$

where  $\lambda_0$  is the chemical potential enforcing the constraint exactly. Here, we implicitly sum over  $\sigma$  and  $\alpha$ .

The model (21) shows a transition driven by variation of  $\varepsilon_0 = \varepsilon_s - \varepsilon_q$ . At the  $\varepsilon_0 = g_0 = 0$  fixed point, tree-level scaling analysis shows that

$$\dim[g_0] = \frac{1-r}{2} \equiv \bar{r}, \quad \dim[\varepsilon_0] = 1. \quad (22)$$

As in the single-channel model,<sup>20,21</sup> this establishes the role of  $r = 1$  as an upper critical dimension where  $g_0$  is marginal.

We perform a field-theoretical RG analysis using the minimal subtraction scheme.<sup>43,44</sup> Renormalized fields and dimensionless couplings are introduced according to

$$f_{\sigma} = \sqrt{Z_f} f_{R\sigma}, \quad (23)$$

$$b_{\bar{\alpha}} = \sqrt{Z_b} b_{R\bar{\alpha}}, \quad (24)$$

$$g_0 = \frac{\mu^{\bar{r}} Z_g}{\sqrt{Z_f Z_b}} g, \quad (25)$$

where  $\mu$  is the renormalization group energy scale. No renormalizations are needed for the bulk fermions as their self-interaction is assumed to be irrelevant. The RG is conveniently performed at criticality, i.e., we assume that  $\varepsilon_0$  is tuned to the critical line and set  $\varepsilon_q = \varepsilon_s = 0$ .

To determine the RG  $\beta$  function  $\beta(g)$  we evaluate the fermionic self-energy up to one-loop order,

$$\Sigma_{f_{\sigma}}(i\omega_n) = K g^2 \frac{\mu^{2\bar{r}}}{\beta} \sum_{i\omega'_n} \int_{-\Lambda}^{\Lambda} dk |k|^r \frac{1}{i\omega'_n - k} \frac{1}{i\bar{\omega}_n - i\omega'_n}, \quad (26)$$

corresponding to the diagram in Fig. 8(a). Here, we have introduced the abbreviated notation  $i\bar{\omega}_n = i\omega_n - \lambda_0$  for the Matsubara frequencies  $i\omega_n = i\pi(2n+1)/\beta$ . In the limit  $\lambda_0 \rightarrow \infty$  and  $\beta \rightarrow \infty$  we obtain

$$\Sigma_{f_{\sigma}}(i\omega_n) = K g^2 \mu^{2\bar{r}} \int_0^{\Lambda} d\epsilon \epsilon^r \frac{1}{i\bar{\omega}_n - \epsilon} \quad (27)$$

$$\approx -K g^2 \left( \mu^{2\bar{r}} \frac{\Lambda^r}{r} + i\bar{\omega}_n \frac{1}{2\bar{r}} \right). \quad (28)$$

An analogous expression is found for the bosonic self-energy  $\Sigma_{b_{\bar{\alpha}}}$  depicted in Fig. 8(b).



FIG. 8. Feynman diagrams entering the self-energies up to quadratic order in  $g_0$ . Full, dashed, and wiggly lines denote  $f_{\sigma}$ ,  $c_{\sigma}$ , and  $b_{\bar{\alpha}}$  propagators, respectively; the full dots are  $g_0$  interaction vertices.

The renormalization factors are determined such that they cancel the  $\frac{1}{2\bar{r}}$  pole in the self-energies minimally and render finite the inverse Green's function. We thus find

$$Z_f = 1 - K \frac{g^2}{2\bar{r}}, \quad Z_b = 1 - N \frac{g^2}{2\bar{r}}. \quad (29)$$

The mass counterterms are given by the real parts of the self-energies,

$$\delta\lambda_f = K g^2 \mu^{2\bar{r}} \frac{\Lambda^r}{r}, \quad \delta\lambda_b = N g^2 \mu^{2\bar{r}} \frac{\Lambda^r}{r}. \quad (30)$$

To one-loop order, there is no vertex renormalization of  $g$ ; hence we have  $Z_g = 1$  at this order (note that a  $g^3$  diagram does not exist due to the directed nature of the propagators). The  $\beta$  function

$$\beta(g) \equiv \mu \frac{dg}{d\mu} \quad (31)$$

can now be obtained by taking the logarithmic  $\mu$  derivative of Eq. (25). Since  $\mu \frac{dg_0}{d\mu} = 0$  we can solve for  $\beta(g)$  and finally obtain

$$\beta(g) = -\frac{1-r}{2} g + \frac{K+N}{2} g^3 \quad (32)$$

to one-loop order. One can also consider the flow away from criticality, i.e., the flow of the renormalized tuning parameter  $\varepsilon$  using  $S^2$  insertions. The resulting correlation-length exponent is given in Eq. (38) below.

### C. $r_{\max} < r < 1$

For  $r < 1$  the trivial fixed point  $g^* = 0$  is unstable, and the critical properties are instead controlled by an interacting fixed point (labeled ACR) at

$$g^{*2} = \frac{1-r}{K+N} \quad (33)$$

with anomalous field dimensions

$$\eta_b = \beta(g) \left. \frac{d \ln Z_b}{dg} \right|_{g^*} = N g^{*2}, \quad (34)$$

$$\eta_f = \beta(g) \left. \frac{d \ln Z_f}{dg} \right|_{g^*} = K g^{*2}. \quad (35)$$

The corresponding RG flow diagram is displayed in Fig. 2(c).

ACR describes a quantum phase transition below its upper critical dimension. As a result, low-energy observables calculated at and near ACR will be fully universal, i.e., cutoff independent, and hyperscaling is fulfilled.

### D. $r \geq 1$

For all  $r \geq 1$ , i.e., above the upper critical dimension, the phase transition between LM and LM' is now controlled by the

noninteracting FImp fixed point at  $g = \varepsilon = 0$ . Hence, for all  $r > 1$  the phase transition is a level crossing with perturbative corrections—this results, e.g., in a jump of the order parameter  $T\chi_{\text{loc}}$  (see below), i.e., the transition is formally of first order. Consequently, hyperscaling is violated, and all observables depend upon the UV cutoff.

For the marginal case,  $r = 1$ , we expect a logarithmic flow of the marginally irrelevant hybridization  $g$ , characteristic of the behavior at the upper critical dimension. The RG  $\beta$  function

$$\beta(g) = \frac{K + N}{2} g^3 \quad (36)$$

can be integrated [recall that  $\beta(g) \equiv \frac{dg}{d \ln \ell}$  where  $\ell$  describes the reduction of the UV cutoff  $\Lambda \rightarrow \ell \Lambda$ ] to give

$$g^2(\ell) = \frac{g_0^2}{1 - (K + N)g_0^2 \ln \ell} \quad (37)$$

with  $g(\ell=1) = g_0$ . This result can be used to determine logarithmic corrections to observables.

## E. Observables near criticality

### 1. Correlation-length exponent

We start with the correlation-length exponent  $\nu$  of the ACR fixed point. This exponent describes the vanishing of the characteristic crossover temperature in the vicinity of the critical point  $T^* \propto (\varepsilon - \varepsilon^*)^\nu$ . The lowest-order result for  $\nu$ , which can be obtained either using the field-theoretic RG scheme via composite operator insertions or using the familiar momentum shell scheme, is

$$\frac{1}{\nu} = r + O(\bar{r}^2) \quad (r < 1). \quad (38)$$

For  $r \geq 1$  the transition is a level crossing, formally  $\nu = 1$ .

### 2. Local susceptibility

The local susceptibility  $\chi_{\text{loc}} = \chi_{\text{imp,imp}}$  at the critical point follows the scaling behavior  $\chi_{\text{loc}} \propto T^{-1+\eta_\chi}$  with an anomalous exponent  $\eta_\chi$ . To obtain the corrections to the tree-level result  $\chi_{\text{loc}} \propto T^{-1}$ , we introduce a  $\chi_{\text{loc}}$  renormalization factor  $Z_\chi$  from which one obtains the anomalous exponent according to

$$\eta_\chi = \beta(g) \left. \frac{d \ln Z_\chi}{dg} \right|_{g^*}. \quad (39)$$

We determine  $Z_\chi$  by calculating  $\langle \chi_{\text{loc}} \rangle$  directly using perturbative corrections up to quadratic order in  $g_0$ . The corresponding diagrams entering  $\langle \chi_{\text{loc}} \rangle_{\lambda_0}$  are given in Fig. 9. In terms of the

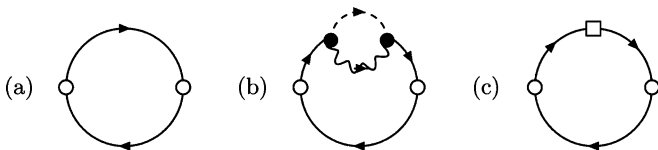


FIG. 9. Feynman diagrams entering  $\langle \chi_{\text{loc}} \rangle_{\lambda_0}$  up to quadratic order in  $g_0$ . Open circles are sources, and blank boxes denotes the counterterms  $\delta\lambda_f$ . Notation otherwise as in Fig. 8

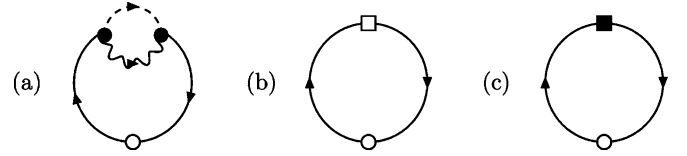


FIG. 10. Feynman diagrams entering the corrections to the unperturbed part of  $\langle \hat{Q} \rangle_{\lambda_0}$  up to quadratic order in  $g_0$ . Notation as in the previous figures. Black boxes denote the counterterms  $\delta\lambda_b$ .

renormalized coupling constant  $g$  we find at the energy scale  $\mu = T$

$$\langle \chi_{\text{loc}} \rangle_{\lambda_0} = e^{-\lambda_0/T} \left( \frac{1}{2T} + \frac{Kg^2}{T} \int_0^{\Lambda/T} dx \frac{x^r}{x^3} \left[ 2 \tanh \frac{x}{2} + \frac{x^2}{2} \tanh \frac{x}{2} - x - \frac{x^2}{2} \right] \right). \quad (40)$$

Furthermore, the denominator  $\langle \hat{Q} \rangle_{\lambda_0}$  receives corrections from the diagrams in Fig. 10, resulting in

$$\langle \hat{Q} \rangle_{\lambda_0} = (N + K)e^{-\lambda_0/T} + 2NKg^2 e^{-\lambda_0/T} \times \int_0^{\Lambda/T} dx \frac{x^r}{x} \left[ \tanh \frac{x}{2} - 1 \right]. \quad (41)$$

The local susceptibility  $\chi_{\text{loc}}$  can then be directly obtained by Eq. (19). The renormalization factor  $Z_\chi$  is then determined, using minimal subtraction of poles, in an expansion in  $\bar{r}$  as

$$Z_\chi = 1 - Kg^2 \frac{1}{\bar{r}}, \quad (42)$$

and from this we can directly deduce the anomalous exponent of the local spin susceptibility,

$$\eta_\chi^{(\text{spin})} = 2Kg^{*2} = \frac{2K}{K+N}(1-r). \quad (43)$$

The expression for  $\eta_\chi^{(\text{flavor})}$  follows by the replacement  $K \leftrightarrow N$ .

Above the upper critical dimension,  $r > 1$ , we simply have  $\eta_\chi = 0$  and, thus,  $\chi_{\text{loc}}^{(\text{spin})}, \chi_{\text{loc}}^{(\text{flavor})} \propto T^{-1}$  or  $\propto \omega^{-1}$ . For the marginal case  $r = 1$ , a calculation analogous to that in Ref. 21, using Eq. (37), gives

$$\chi_{\text{loc}}^{(\text{spin})} \propto \frac{1}{\omega |\ln \omega|^{2K/(K+N)}} \quad (r = 1). \quad (44)$$

### 3. Order parameter

Inside the stable phases LM and LM',  $\chi_{\text{loc}}$  can be used to define an order parameter for the quantum phase transition:  $T\chi_{\text{loc}}^{\text{spin}}$  is finite (zero) for  $\varepsilon_0 < 0$  ( $\varepsilon_0 > 0$ ), and similarly  $T\chi_{\text{loc}}^{\text{flavor}}$  is finite (zero) for  $\varepsilon_0 > 0$  ( $\varepsilon_0 < 0$ ). On approach to the critical point, both order parameters vanish continuously according to

$$T\chi_{\text{loc}}^{(\text{spin})} \propto (-\varepsilon_0)^{\nu\eta_\chi^{(\text{spin})}}, \quad T\chi_{\text{loc}}^{(\text{flavor})} \propto \varepsilon_0^{\nu\eta_\chi^{(\text{flavor})}} \quad (45)$$

for  $r < 1$ , which follows, e.g., from hyperscaling. Note that these order parameters display a jump upon crossing the transition for  $r > 1$ .

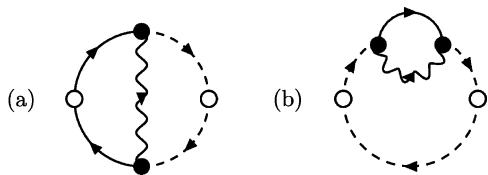


FIG. 11. Further Feynman diagrams entering corrections to the impurity susceptibility to quadratic order in  $g_0$ . Notation as in the previous figures.

#### 4. Impurity susceptibility

The evaluation of the impurity susceptibility  $\chi_{\text{imp}}$  to second order in  $g_0$  requires the summation of further diagrams as depicted in Fig. 11. In terms of the renormalized coupling  $g$  we obtain

$$2\langle\chi_{\text{b,imp}}\rangle_{\lambda_0} = \frac{Kg^2}{T}e^{-\lambda_0/T} \int_0^{\Lambda/T} dx \frac{x^r}{x^3} \left[ x + \frac{x}{\cosh^2 \frac{x}{2}} - 4 \tanh \frac{x}{2} \right] \quad (46)$$

and

$$\langle\chi_{\text{b,b}}\rangle_{\lambda_0} - \langle\chi_{\text{b,b}}^0\rangle_{\lambda_0} = \frac{Kg^2}{T}e^{-\lambda_0/T} \int_0^{\Lambda/T} dx \frac{x^r}{x^3} \times \left[ 2 \tanh \frac{x}{2} - \frac{x}{\cosh^2 \frac{x}{2}} - \frac{x^2 \tanh \frac{x}{2}}{2 \cosh^2 \frac{x}{2}} \right]. \quad (47)$$

Collecting all contributions to  $\chi_{\text{imp}}$  to second order in  $g$ , the poles present in the  $\chi_{\text{loc}}$  diagrams cancel and the remaining momentum integrals are UV convergent for  $r < 1$ . On performing these integrals for  $r < 1$ , the impurity susceptibility reads

$$T\chi_{\text{imp}}^{(\text{spin})} = \frac{1}{2(N+K)} \left[ 1 - g^2 K \left( 1 + \ln 4 - \frac{2N}{N+K} \ln 4 \right) \right] + O(g^4). \quad (48)$$

As above, the expression for  $T\chi_{\text{imp}}^{(\text{flavor})}$  follows by the replacement  $K \leftrightarrow N$ . With the value of the coupling at the ACR fixed point (33), we finally find for  $N = K = 2$ , to leading order in  $(1-r)$ ,

$$T\chi_{\text{imp}}^{(\text{spin})} = \begin{cases} \frac{1}{8} - \frac{1}{16}(1-r) + O(\bar{r}^2) & (r < 1), \\ \frac{1}{8} & (r \geq 1), \end{cases} \quad (49)$$

with  $T\chi_{\text{imp}}^{(\text{flavor})} = T\chi_{\text{imp}}^{(\text{spin})}$  due to the emergent  $Z_2$  symmetry (4). A comparison to NRG data is in Fig. 3. Note that  $T\chi_{\text{imp}}$  receives only weak additive logarithmic corrections at  $r = 1$ ; multiplicative logarithms as in  $\chi_{\text{loc}}$  are absent here. The same applies to  $S_{\text{imp}}$  below.

#### 5. Impurity entropy

The impurity contribution to the entropy can be obtained from the thermodynamic potential  $\Omega_{\text{imp}}$  by  $S_{\text{imp}} = -\partial_T \Omega_{\text{imp}}$ . At the FImp fixed point the entropy is  $S_{\text{imp}} = \ln(N+K)$ , and the lowest-order correction is computed by expanding the

thermodynamic potential in the renormalized hybridization  $g$ . Note that this correction vanishes for  $r \geq 1$ , as  $g^* = 0$  there. Here, we write the partition function in the physical sector of the Hilbert space ( $\hat{Q} = 1$ ) as<sup>37</sup>

$$\frac{Z_{\text{imp}}}{Z_{\text{imp},0}} = \lim_{\lambda_0 \rightarrow \infty} \frac{\langle \hat{Q} \rangle_{\lambda_0}}{\langle \hat{Q} \rangle_{\lambda_0,0}}, \quad (50)$$

where  $\langle \cdots \rangle_{\lambda_0,0}$  is the expectation value in the presence of  $\lambda_0$  without coupling to the bath. The thermodynamic potential is given by

$$\Omega_{\text{imp}} - \Omega_{\text{imp},0} = -T \ln \frac{Z_{\text{imp}}}{Z_{\text{imp},0}}. \quad (51)$$

The correction to  $\langle \hat{Q} \rangle_{\lambda_0}$  due to the coupling to the bath up to quadratic order in  $g$  has already been calculated in Eq. (41), which enables us now to directly evaluate Eq. (51). Taking the temperature derivative of the resulting expression and evaluating the remaining integral in the limit  $T \rightarrow 0$  and  $r \rightarrow 1$ , we obtain

$$S_{\text{imp}} = \ln(K+N) - g^2 \frac{4NK}{N+K} \ln 2 + O(g^4). \quad (52)$$

As expected, the entropy correction is fully universal and finite in the limit  $T \rightarrow 0$ . Note that in higher-order terms of the diagrammatic expansion for the thermodynamic potential  $\Omega_{\text{imp}}$  disconnected diagrams appear.<sup>37</sup>

Finally, inserting the fixed-point value of the coupling  $g$  into Eq. (52), we find the impurity entropy in the two-channel case  $N = 2$  and  $K = 2$  to be

$$S_{\text{imp}} = \begin{cases} \ln 4 - (1-r) \ln 2 + O(\bar{r}^2) & (r < 1), \\ \ln 4 & (r \geq 1). \end{cases} \quad (53)$$

Comparison with the numerical result again shows very good agreement, Fig. 4.

#### 6. Conduction-electron $T$ matrix

For the single-channel pseudogap Kondo problem, it has been shown that the conduction-electron  $T$  matrix  $T(\omega)$  displays a power-law divergence of the form  $T(\omega) \propto |\omega|^{-r}$  at all intermediate-coupling fixed points.<sup>20,21</sup> Analytically, this follows—for all perturbative expansions—from the diagrammatic structure of the  $T$  matrix (or, alternatively, from a Ward identity).

In the two-channel case, we find that the same qualitative arguments apply, i.e., at the NFL, SCR, and ACR fixed points the  $T$  matrix obeys the exact result

$$T(\omega) \propto |\omega|^{-r} \quad (r < 1). \quad (54)$$

At one-loop level, an explicit calculation gives  $\eta_T = (K+N)g^2$ , which yields  $\eta_T = 1-r$  as expected. For  $r > 1$ ,  $\text{Im} T(\omega) \propto \delta(\omega)$ .

For  $r = 1$ , the logarithmic flow of the coupling, Eq. (37), can be used to deduce  $T(\omega) \propto 1/(\omega |\ln \omega|)$ , which gives

$$\text{Im} T(\omega) \propto \frac{1}{\omega |\ln \omega|^2} \quad (r = 1), \quad (55)$$

in analogy to Ref. 21.

## VI. CONCLUSIONS

We have explored the two-channel Kondo effect for magnetic impurities embedded into a fermionic host with a power-law pseudogapped density of states. We have determined the phase diagram as a function of the DOS exponent  $r$  and discussed the boundary quantum phase transitions of the relevant Kondo and Anderson models. These transitions are described by fermionic (as opposed to the usual bosonic) quantum field theories; from their properties we conclude that there is no underlying CFT description.

Our results demonstrate the versatility of the Anderson-model  $\epsilon$  expansions developed in Refs. 20 and 21: Those have allowed a full understanding not only of the critical behavior of the single-channel ( $S = 1/2$ ) pseudogap Kondo problem, but also of the corresponding underscreened<sup>47</sup> and overscreened pseudogap Kondo models (this work). Further applications, e.g., to multi-impurity models, appear possible. Also, the Anderson model formulation should enable studies of nonequilibrium dynamics of pseudogap Kondo problems.

Our results are of potential relevance to two-channel impurities in unconventional superconductors and in graphene; for the latter case the extension of the present calculations to finite bias<sup>48</sup> is an interesting future topic.

## ACKNOWLEDGMENTS

We thank A. J. Schofield and, in particular, K. Ingersent for helpful discussions. This research has been supported by the Deutsche Forschungsgemeinschaft through SFB 608 (L.F.), FOR 960 (A.B., M.V.), and AN 275/6-2 (F.B.A.). F.B.A. and M.V. also acknowledge support from the German-Israeli Foundation.

## APPENDIX: COMPACTIFIED $\sigma$ - $\tau$ KONDO MODEL AND O(3)-SYMMETRIC ANDERSON MODEL

Here we briefly discuss an alternative formulation of the two-channel Kondo model which eventually leads to a theory of noninteracting Majorana fermions.

### 1. Metallic bath, $r = 0$

The low-energy physics of the standard two-channel Kondo problem ( $r = 0$ ) has been argued to be equivalent to that of the so-called  $\sigma$ - $\tau$  Kondo model—this is a “compactified” single-channel Kondo model where the roles of the two screening channels are taken by spin and a charge pseudospin.<sup>49,50</sup> The corresponding Hamiltonian can be expressed as

$$\mathcal{H}_{\sigma-\tau} = [J_1 \vec{\sigma}(0) + J_2 \vec{\tau}(0)] \cdot \vec{S} + \int_{-\Lambda}^{\Lambda} dk k c_{k\sigma}^\dagger c_{k\sigma}, \quad (\text{A1})$$

where, as above,  $\vec{S}$  is a spin-1/2 SU(2) spin and we have represented the bath by linearly dispersing chiral fermions  $c_{k\sigma}$ . Spin degrees of freedom  $\sigma = \uparrow, \downarrow$  are implicitly summed. The conduction-electron spin  $\vec{\sigma}(0)$  and pseudospin  $\vec{\tau}(0)$  are defined as

$$\vec{\sigma}(0) = (c_{\uparrow}^\dagger(0), c_{\downarrow}^\dagger(0)) \cdot \vec{\tau} \cdot \begin{pmatrix} c_{\uparrow}(0) \\ c_{\downarrow}(0) \end{pmatrix}, \quad (\text{A2})$$

$$\vec{\tau}(0) = (c_{\uparrow}^\dagger(0), c_{\downarrow}(0)) \cdot \vec{\tau} \cdot \begin{pmatrix} c_{\uparrow}(0) \\ c_{\downarrow}^\dagger(0) \end{pmatrix}, \quad (\text{A3})$$

where  $c_{\sigma}(0) = \int dk c_{k\sigma}$ . Interestingly, the low-energy physics of the  $\sigma$ - $\tau$  Kondo model is described by a fixed point with non-Fermi-liquid behavior which is located at *strong* coupling, not at intermediate coupling as in the two-channel Kondo problem. The equivalence of the two-channel Kondo model and the  $\sigma$ - $\tau$  Kondo model has been established using bosonization and conformal field theory techniques.<sup>49–51</sup>

The nature of the low-energy non-Fermi liquid becomes transparent by considering the so-called O(3)-symmetric Anderson model which displays an anomalous hybridization term. Its Hamiltonian is given by  $\mathcal{H}_{O(3)} = \mathcal{H}_{1cA} + \mathcal{H}_{\text{ahyb}}$  with

$$\begin{aligned} \mathcal{H}_{1cA} &= U \left( n_{f\uparrow} - \frac{1}{2} \right) \left( n_{f\downarrow} - \frac{1}{2} \right) \\ &+ \int_{-\Lambda}^{\Lambda} dk k c_{k\sigma}^\dagger c_{k\sigma} + g_0 \sum_{\sigma} [f_{\sigma}^\dagger c_{\sigma}(0) + \text{H.c.}], \quad (\text{A4}) \end{aligned}$$

$$\mathcal{H}_{\text{ahyb}} = -g_a [f_{\downarrow}^\dagger c_{\downarrow}^\dagger(0) + f_{\downarrow}^\dagger c_{\downarrow}(0) + \text{H.c.}], \quad (\text{A5})$$

where  $f_{\sigma}^\dagger$  creates the localized impurity state with spin  $\sigma$  and  $n_{f\sigma} = f_{\sigma}^\dagger f_{\sigma}$ . Note that the chemical potential on the impurity site has been chosen such that the model is p-h symmetric. In the Kondo limit, the O(3)-symmetric Anderson model maps onto the  $\sigma$ - $\tau$  Kondo model.<sup>51</sup>

Consideration of the adiabatic continuity between the  $U = 0$  and large- $U$  limits in this Anderson model suggests discussion of the weakly interacting case. The Hamiltonian  $\mathcal{H}_{O(3)}$  can be conveniently rewritten in terms of Majorana fermions:

$$\begin{aligned} \mathcal{H}_{O(3)} &= U d_1 d_2 d_3 d_0 + i \sum_{\alpha=0}^3 \int_{-\Lambda}^{\Lambda} dk k \psi_{-k\alpha} \psi_{k\alpha} \\ &+ i g_0 \sum_{\alpha=1}^3 \psi_{\alpha}(0) d_{\alpha} + i (g_0 - 2g_a) \psi_0(0) d_0. \quad (\text{A6}) \end{aligned}$$

Here, the impurity Majorana fermions are defined by

$$f_{\uparrow} = \frac{1}{\sqrt{2}}(d_1 - i d_2), \quad f_{\downarrow} = \frac{1}{\sqrt{2}}(-d_3 + i d_0), \quad (\text{A7})$$

where  $d_{\alpha}^{\dagger} = d_{\alpha}$  and  $\{d_{\alpha}, d_{\beta}\} = \delta_{\alpha, \beta}$  for  $\alpha = 0, 1, 2, 3$ . The Majorana fermions for the conduction electrons are defined similarly;<sup>51</sup> in Fourier space they read

$$c_{k\uparrow} = \frac{1}{\sqrt{2}}(-i\psi_{k1} - \psi_{k2}), \quad c_{k\downarrow} = \frac{1}{\sqrt{2}}(i\psi_{k3} - \psi_{k4}) \quad (\text{A8})$$

with  $\psi_{k\alpha}^{\dagger} = \psi_{-k\alpha}$ . Remarkably, for  $2g_a = g_0$  the impurity couples only via  $d_{\alpha}$  for  $\alpha = 1, 2, 3$  to the conduction Majorana fermions while  $d_0$  remains free.

The Hamiltonian in Eq. (A6) is suitable to study thermodynamic quantities in particular. Note that for  $U = 0$  the model is exactly solvable and the impurity Green's functions  $G_{\alpha}(\tau) = -\langle T_{\tau} d_{\alpha}(\tau) d_{\alpha}(0) \rangle$  are known exactly. For  $U = 0$  and  $2g_a = g_0$ , their Fourier counterparts read

$$G_0(i\omega_n) = \frac{1}{i\omega_n}, \quad G_{\alpha}(i\omega_n) = \frac{1}{i\omega_n + iA_0 \text{sgn}(\omega_n)}, \quad (\text{A9})$$

for  $\alpha = 1, 2, 3$ . Here, we have introduced  $A_0 = \pi g_0^2$ .

A straightforward calculation now shows that there is a residual impurity entropy  $S_{\text{imp}} = \frac{1}{2} \ln 2$  of a free Majorana fermion.<sup>52</sup> By adiabatic continuity, this entropy persists into the regime of large  $U$  and then corresponds to the entropy of the overscreened two-channel Kondo impurity.

## 2. Pseudogap bath

The obvious question is whether the  $\sigma$ - $\tau$  Kondo and O(3)-symmetric Anderson models continue to represent the physics of the two-channel Kondo problem for a pseudogap bath DOS with  $r > 0$ . To answer this, let us consider the noninteracting limit and  $2g_a = g_0$  of the O(3) Anderson model. The Green's functions in Eq. (A9) for  $\omega_n/\Lambda \ll 1$  are now given by<sup>21</sup>

$$G_0(i\omega_n) = \frac{1}{i\omega_n}, \quad (\text{A10})$$

$$G_\alpha(i\omega_n) = \frac{1}{i\omega_n + iA_0 \text{sgn}(\omega_n)|\omega_n|^r} \quad (\text{A11})$$

for  $\alpha = 1, 2, 3$ . They yield an impurity entropy of

$$S_{\text{imp}} = \frac{1}{2} \ln 2 + \frac{3}{2} r \ln 2 \quad (\text{A12})$$

and an impurity susceptibility of

$$T \chi_{\text{imp}}(T) = \frac{3r}{32}. \quad (\text{A13})$$

This result is not in agreement with the numerical data in Figs. 3 and 4, which instead are well fitted by  $S_{\text{imp}} = \frac{1}{2} \ln 2 + 2r \ln 2$  and  $T \chi_{\text{imp}}(T) = \frac{r}{6}$  (Ref. 19). We are forced to conclude that the low-energy behavior of the  $\sigma$ - $\tau$  Kondo and O(3)-symmetric Anderson models is *not* identical to that of the two-channel Kondo model once  $r > 0$ . In other words, the equivalence is restricted to the metallic  $r = 0$  case. Given the fact that neither bosonization nor CFT appears to be applicable to the pseudogap Kondo models, this may not come as a surprise.

Let us finish with the remark that an extension of the Majorana resonant-level model that corresponds to the solvable point of the two-channel Kondo model<sup>7</sup> to a pseudogap DOS also does not yield the numerically found impurity entropy.

<sup>1</sup>P. Nozières and A. Blandin, *J. Phys. (Paris)* **41**, 193 (1980).

<sup>2</sup>N. Andrei and C. Destri, *Phys. Rev. Lett.* **52**, 364 (1984).

<sup>3</sup>P. B. Wiegmann and A. M. Tsvelik, *Z. Phys. B* **54**, 201 (1985).

<sup>4</sup>I. Affleck and A. W. W. Ludwig, *Nucl. Phys. B* **352**, 849 (1991); **360**, 641 (1991).

<sup>5</sup>A. W. W. Ludwig and I. Affleck, *Phys. Rev. Lett.* **67**, 3160 (1991).

<sup>6</sup>E. Sela, A. K. Mitchell, and L. Fritz, *Phys. Rev. Lett.* **106**, 147202 (2011).

<sup>7</sup>V. J. Emery and S. Kivelson, *Phys. Rev. B* **46**, 10812 (1992).

<sup>8</sup>D. L. Cox and A. Zawadowski, *Adv. Phys.* **47**, 599 (1998).

<sup>9</sup>D. L. Cox, *Phys. Rev. Lett.* **59**, 1240 (1987); **61**, 1527(E) (1988).

<sup>10</sup>A. Schiller, F. B. Anders, and D. L. Cox, *Phys. Rev. Lett.* **81**, 3235 (1998).

<sup>11</sup>R. M. Potok, I. G. Rau, H. Shtrikman, Y. Oreg, and D. Goldhaber-Gordon, *Nature (London)* **446**, 167 (2007).

<sup>12</sup>Y. Oreg and D. Goldhaber-Gordon, *Phys. Rev. Lett.* **90**, 136602 (2003).

<sup>13</sup>H. C. Manoharan *et al.* (unpublished).

<sup>14</sup>A. C. Hewson, *The Kondo Problem to Heavy Fermions* (Cambridge University Press, Cambridge, 1997).

<sup>15</sup>D. Withoff and E. Fradkin, *Phys. Rev. Lett.* **64**, 1835 (1990).

<sup>16</sup>C. R. Cassanello and E. Fradkin, *Phys. Rev. B* **53**, 15079 (1996); **56**, 11246 (1997).

<sup>17</sup>A. Polkovnikov, *Phys. Rev. B* **65**, 064503 (2002).

<sup>18</sup>R. Bulla, T. Pruschke, and A. C. Hewson, *J. Phys.: Condens. Matter* **9**, 10463 (1997); R. Bulla, M. T. Glossop, D. E. Logan, and T. Pruschke, *ibid.* **12**, 4899 (2000).

<sup>19</sup>C. Gonzalez-Buxton and K. Ingersent, *Phys. Rev. B* **57**, 14254 (1998).

<sup>20</sup>M. Vojta and L. Fritz, *Phys. Rev. B* **70**, 094502 (2004).

<sup>21</sup>L. Fritz and M. Vojta, *Phys. Rev. B* **70**, 214427 (2004).

<sup>22</sup>K. Sengupta and G. Baskaran, *Phys. Rev. B* **77**, 045417 (2008).

<sup>23</sup>Reference 18 overlooked the slow flow of the particle-hole asymmetry toward zero in the NFL phase for  $0 < r < r_{\text{max}}$  [K. Ingersent (private communication)]. As a result, the phase

diagram in Fig. 30(a) of Ref. 18 differs qualitatively from ours [Fig. 1(b)].

<sup>24</sup>The fixed point LM' was labeled ASC (for asymmetric strong coupling) in Ref. 18.

<sup>25</sup>C. J. Bolech and N. Andrei, *Phys. Rev. Lett.* **88**, 237206 (2002).

<sup>26</sup>H. Johannesson, N. Andrei, and C. J. Bolech, *Phys. Rev. B* **68**, 075112 (2003).

<sup>27</sup>C. J. Bolech and N. Andrei, *Phys. Rev. B* **71**, 205104 (2005).

<sup>28</sup>F. B. Anders, *Phys. Rev. B* **71**, 121101(R) (2005).

<sup>29</sup>G. R. Stewart, Z. Fisk, and J. O. Willis, *Phys. Rev. B* **28**, 172 (1983).

<sup>30</sup>F. G. Aliev, H. El Mfarrej, S. Vieira, R. Villar, and J. L. Martinez, *Europhys. Lett.* **32**, 765 (1995).

<sup>31</sup>K. A. Matveev, *Sov. Phys. JETP* **72**, 892 (1991).

<sup>32</sup>E. Lebanon, A. Schiller, and F. B. Anders, *Phys. Rev. B* **68**, 041311(R) (2003).

<sup>33</sup>O. Parcollet and A. Georges, *Phys. Rev. Lett.* **79**, 4665 (1997); O. Parcollet, A. Georges, G. Kotliar, and A. M. Sengupta, *Phys. Rev. B* **58**, 3794 (1998).

<sup>34</sup>M. Vojta, *Phys. Rev. Lett.* **87**, 097202 (2001).

<sup>35</sup>M. Vojta, *Philos. Mag.* **86**, 1807 (2006).

<sup>36</sup>M. Vojta, C. Buragohain, and S. Sachdev, *Phys. Rev. B* **61**, 15152 (2000).

<sup>37</sup>M. Kirćan and M. Vojta, *Phys. Rev. B* **69**, 174421 (2004).

<sup>38</sup>H. Georgi, *Lie Algebras in Particle Physics* (Westview Press, Boulder, CO, 1999).

<sup>39</sup>R. Bulla, T. A. Costi, and T. Pruschke, *Rev. Mod. Phys.* **80**, 395 (2008).

<sup>40</sup>I. Affleck and A. W. W. Ludwig, *Phys. Rev. Lett.* **67**, 161 (1991).

<sup>41</sup>S. Florens and A. Rosch, *Phys. Rev. Lett.* **92**, 216601 (2004).

<sup>42</sup>P. W. Anderson, *J. Phys. C* **3**, 2436 (1970).

<sup>43</sup>E. Brezin, J. C. Le Guillou, and J. Zinn-Justin, in *Phase Transitions and Critical Phenomena*, edited by C. Domb and (Page Bros., Norwich, UK, 1996), Vol. 6.

- <sup>44</sup>M. Le Bellac, *Quantum and Statistical Field Theory* (Oxford University Press, Oxford, 1992).
- <sup>45</sup>A. Zawadowski and P. Fazekas, *Z. Phys.* **226**, 235 (1969); P. Coleman, *Phys. Rev. B* **29**, 3035 (1984).
- <sup>46</sup>T. A. Costi, J. Kroha, and P. Wölfle, *Phys. Rev. B* **53**, 1850 (1996).
- <sup>47</sup>S. Florens and M. Vojta, *Phys. Rev. B* **72**, 115117 (2005).
- <sup>48</sup>M. Vojta, L. Fritz, and R. Bulla, *EPL* **90**, 27006 (2010).
- <sup>49</sup>P. Coleman and A. J. Schofield, *Phys. Rev. Lett.* **75**, 2184 (1995).
- <sup>50</sup>A. J. Schofield, *Phys. Rev. B* **55**, 5627 (1997).
- <sup>51</sup>R. Bulla, A. C. Hewson, and G. M. Zhang, *Phys. Rev. B* **56**, 11721 (1997).
- <sup>52</sup>G. M. Zhang and A. C. Hewson, *Phys. Rev. B* **54**, 1169 (1996).